Latin American Journal of Solids and Structures
www.lajss.org

Numerical Study on the Structural Performance of Steel Beams with Slant End-plate Connections

Abstract

Thermal effects can be one of the most harmful conditions that any steel structure should expect throughout its service life. To counteract this effect, a new beam, with a capability to dissipate thermally induced axial force by slanting of end-plate connection at both ends, is proposed. The beam was examined in terms of its elastic mechanical behavior under symmetric transverse load in presence of an elevated temperature by means of direct stiffness finite element model. The performance of such connection is defined under two resisting mechanisms; by friction force dissipation between faces of slant connection and by small upward crawling on slant plane. The presented numerical method is relatively easy and useful to evaluate the behavior of the proposed beam of various dimensions at different temperatures. Its applicability is evident through satisfactory results verification with those from experimental, analytical and commercially available finite element software. Based on the good agreement between theoretical and experimental methods, a series of design curves were developed as a safe-practical range for the slant end-plate connections which are depend on the conditions of the connection.

Keywords

Slanted end-plate connection, elevated temperature, symmetric transverse load, direct stiffness finite element model, analytical model.

Farshad Zahmatkesh [a]
Mohd. H. Osman [a]
Elnaz Talebi [b]
Ahmad B.H. Kueh [b]
Mahmood. Md. Tahir [b *]

[a] UTM Forensic Engineering Centre, Universiti Teknologi Malaysia (UTM), 81310 UTM Johor, Malaysia.

[b] UTM Construction Research Centre, Universiti Teknologi Malaysia (UTM-CRC), 81310 UTM Johor, Malaysia,

[*]Mahmoodtahir@utm.my

http://dx.doi.org/10.1590/1679-78252158

Received 24.04.2015
In revised form 10.07.2015
Accepted 11.07.2015
Available online 12.04.2016

1 INTRODUCTION

The search for an economical resistance method to improve the performance of steel structures due to elevated temperature remains a challenging task that captures the interest of structural engineers in recent decades. Commonly employed existing engineering solutions to address temperature related concerns are in the forms of increasing section area, provision of lateral supports (Usmani et al.,

2001), cooling action by air-conditioning and watering (Bailey et al., 1996), and thermal break (Larson and Van Geem, 1987). For better thermal resistance, structural members and connections behaviors at elevated temperature remain the principal subject of study of numerous papers exploring on various issues of structural matters. From 168 tests on compressed steel-hinged bars with elastic thermal elongation restrain, Rodrigues et al. (2000) concluded that thermal axial restraint is essential in the determination of fire resistance. This implies the importance of the consideration of connection or restraining component in structures under thermal loads. At elevated temperatures, the designs used for steel structures can be largely deviated from the normal thermal-free condition (Bradford, 2006). To characterize the behaviors of steels such that a full utilization of their special feature can be executed, Chen and Young (2006) had proposed a stress–strain model that unifies the yield strength, elastic modulus, ultimate strength, and ultimate strain of steel at elevated temperatures for general use. Mourão and E Silva (2007) had pointed out that it is insufficient to rely only on the consideration of reduction in strength and modulus of steel structure in the thermal load environment analyses, even when the heat is uniformly distributed. They suggested that the behavior of the structures including the realistic boundary conditions at high temperatures is required under such condition, indicating the significance of design details for the elevated temperature loading resistance. Takagi and Deierlein (2007), making comparisons using nonlinear finite element simulations, evaluated design equations from the American Institute of Steel Construction (AISC, 2013)and European Committee for Standardization (EC3, 2005) for steel members at elevated temperatures. The EC3 (2005)provisions were exhibited to predict to a small disagreement of within 10%–20% of the simulated finite element results. Conversely, AISC (2013) specification predicts strengths that are up to twice as large, from which modifications had been suggested for improvement. Yin and Wang (2004) presented the numerical modeling of the large deflection behavior of steel beams at elevated temperatures with different elastic axial and rotational restraints at the ends, focusing in particular the response in catenary action. They stressed that high temperature engineering design must take into account the effect of axial forces in the beam on the adjacent structure, including the connections, since the level of axial restraint is of the greatest importance due to its influence in the beam deflection and the catenary force under catenary action. Much effort was therefore devoted also to the investigation of the effect of connecting element on the global steel structural response when exposed to temperature change (Al-Jabri, 2011). Dai et al. (2010) witnessed various failure modes in the results of fire tests simulations of restrained steel beam-column assemblies adopting five different types of joints, signifying the importance of connection type details in thermal load resistance. Simões da Silva et al. (2001) had extended the commonly practiced component method to the prediction of the response of steel joints under fire loading, focusing on a cruciform flush end-plate beam-to-column connection and comparing it to the experimental results obtained under various loading conditions. Realizing that restraint against thermal expansion of the beams can produce large axial forces, Heidarpour and Bradford (2009) presented an elastic analysis of a panel zone in a steel frame at elevated temperatures, joined in a rigid or semi-rigid fashion. Using a simple equilibrium premise, they developed an analytical model that takes into account the shear and flexural deformations of the panel zone. It was found that the main characteristics of the panel zone depend extensively on the thermal regime and the large compressive axial load induced in the connection, which is built-up from the restraint to thermal expan-

sion at initial stages of the thermal loading. In much the same vein, numerical study of beam–column joints under thermal load using numerous types of connections had been carried out by Yang and Tan (2012), from which the static solver remains a more accurate tool compared to that of explicit in obtaining structural response although non-convergence can be an issue when dealing with fracture simulation in the former. They commented that changes in the arrangement of bolts in flush end plate connections can improve the structural performance, and that current acceptance criteria of rotation capacities for steel joints are somewhat too conservative as they only consider pure flexural resistance. Accordingly, new connection acceptance criteria were proposed. In addition to available numerical works, Qian et al. (2008) conducted an experimental investigation of steel extended end-plate beam-to-column joints at elevated temperatures at 400, 550, and 700°C with different axial compression forces applied to the beams to simulate restraint effects. It was observed that axial restraint force plays a principal role on the steel joint moment capacity, and that there was a clear beam web tension field action near the column in thermally unrestrained cruciform tests. The fundamental development of an analytical model of such a connection when subjected to a non-symmetric gravity load and a temperature increase has been formulated by Zahmatkesh et al. (2014b). It was demonstrated from the study that an increase in temperature in the beam with a general vertical bolted connection induces a huge extra axial force that decreases the capability in carrying external gravity loads. Also, this study showed that by changing the connection to that of slanting type, this additional axial force can be damped efficiently.

These literatures have clearly identified that the chief concern in steel structures under thermal load lies in the connection details and restraining method. It is worthwhile to note that most existing studies on steel beams have only considered the structural response in the use of conventional vertical end-plate connection due to applied thermal axial forces. So far, there is little evidence that suggests a structural method to reduce the amount of axial force in restrained beams when subjected to elevated temperature. Also, there has been no controlled study comparing differences in the thermal responses of vertical (conventional) and slanted end-plate connections for steel beams.

In the present work, we therefore explore further by means of direct stiffness method the thermal behavior of the slanted end-plate connections in offering the structural solution to protect the beam and connections against primary failure due to elevated temperature. In the spirit of the finding by reference Zahmatkesh et al. (2014a), a 1D direct stiffness finite element method is presented in the current work to examine the behaviors of beams with a slant end-plate connection in the presence of an elevated temperature when subjected to a symmetric transverse load in the elastic regime. In addition to complement the existing analytical solution, this numerical model offers potential to be extended to structures of continuous system with multiple degrees of freedom. In many fire accidents, axially restrained beams are partially or fully yielded before temperature goes to higher than 100° C (elastic) simply due to thermal expansion and axially exerted forces. The current research proposed the slant end-plate connections instead of conventional connections to increase safety of structures for extended heating exposure time for fire fighting. On this basis, the findings from the current paper are useful and applicable for the early occurrence of fire incidents.

2 VERTICAL AND SLANT END-PLATE CONNECTION CHARACTERISTICS OF BEAM SUBJECTED TO TEMPERATURE INCREASE

Figures 1 and 2 show the structural arrangements of vertical and test scale of slant end-plate connection systems respectively. The popularity of bolted end-plate connections is largely due to its simplicity in fabrication and installation. In general, these connections consist of end-plates that are welded to the ends of a beam in the workshop and then bolted to the flange of columns on site. They are usually used in industrial structures, residential towers in terms of knee connections with end-plate and beam connections in gable roofs. The maximum angle of slanting end-plate connection (Figure 2) has been set to 60°, because a higher angle is not practical for crossing bolts into the holes at the top and bottom of end-plate for fastening (Zahmatkesh et al., 2014c).



Figure 1: Steel beam system with vertical bolted end-plate connections.

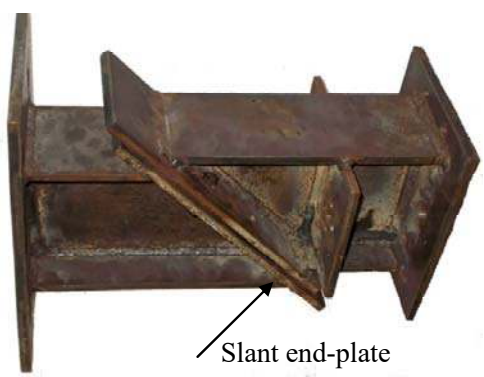

Figure 2: A steel beam system with slant bolted end-plate connections.

The beam with restrained supports tends to have expansion when it is subjected to temperature increase. So, if the supports do not allow enough tolerance for motion, their reactions will apply huge axial forces in the beam. Most of the times, elongation of members in the elastic regime of material is small. Therefore, the introduction of the slant end-plate connection can damp the existing axial force by allowing the ends of beam to crawl on the connection surface due to elongation of the beam. Hypotheses about the stages of the performance and the reaction of end-plate connections due to increase in temperature are shown in Figures 3 and 4, for vertical and slant types, respectively. As shown in Figure 3, after an increase in temperature, the beam generally tends to buckle due to increase in axial load (P_{cr}), because vertical end-plate connection does not allow the beam to have expansion. On the other hand, as shown in Figure 4, the supports reactions apply axial forces after temperature increase to the beam through member expansion such that the slant surface allows the beam to damp axial force and expansion by means of linear crawling on the slant surface. Although there is a vertical motion tolerance between the surfaces in vertical end-plate connections, it is unable to absorb the expansion of two ends of the beam in the horizontal direction because the direction of expansion is perpendicular to the direction of moving surface. In the slant end-plate connection, there is a slanting tolerance between the surfaces such that it can absorb the expansion of two ends of the beam using crawling mechanism over the slanting faces, because the direction of horizontal expansion can be propelled to the slanting plane of connection.

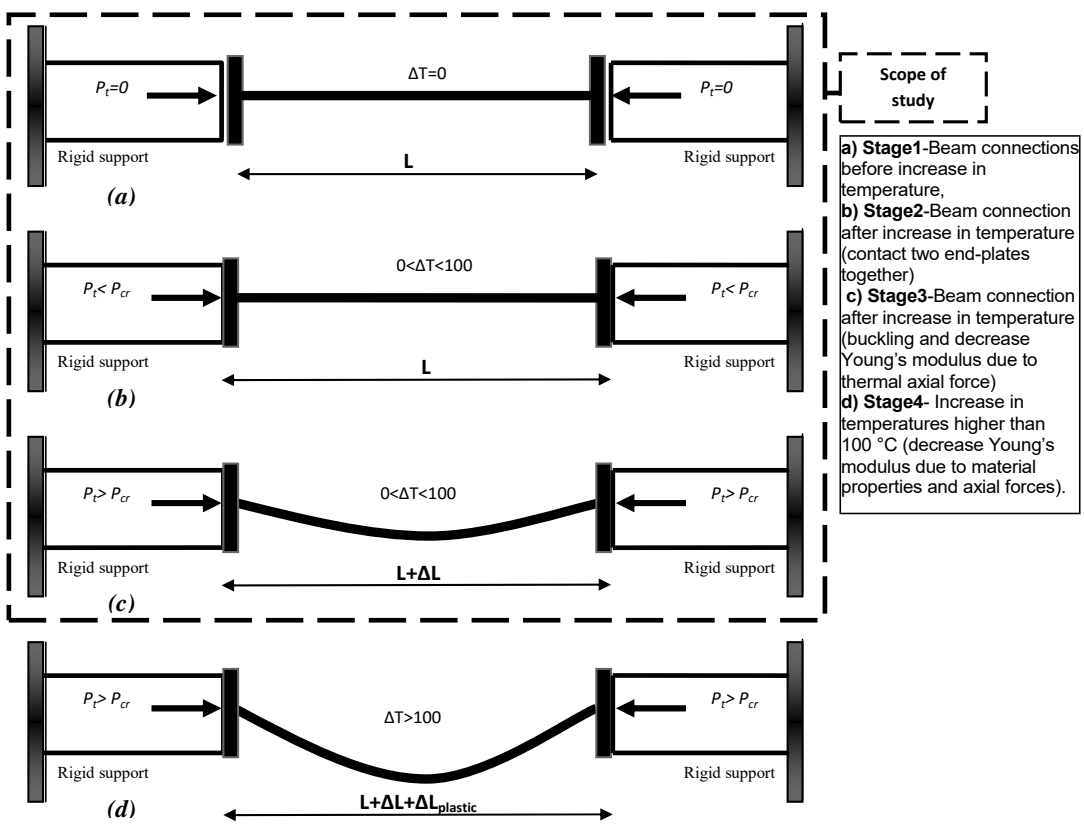

Figure 3: Beam with vertical end-plate connection subjected to temperature increase.

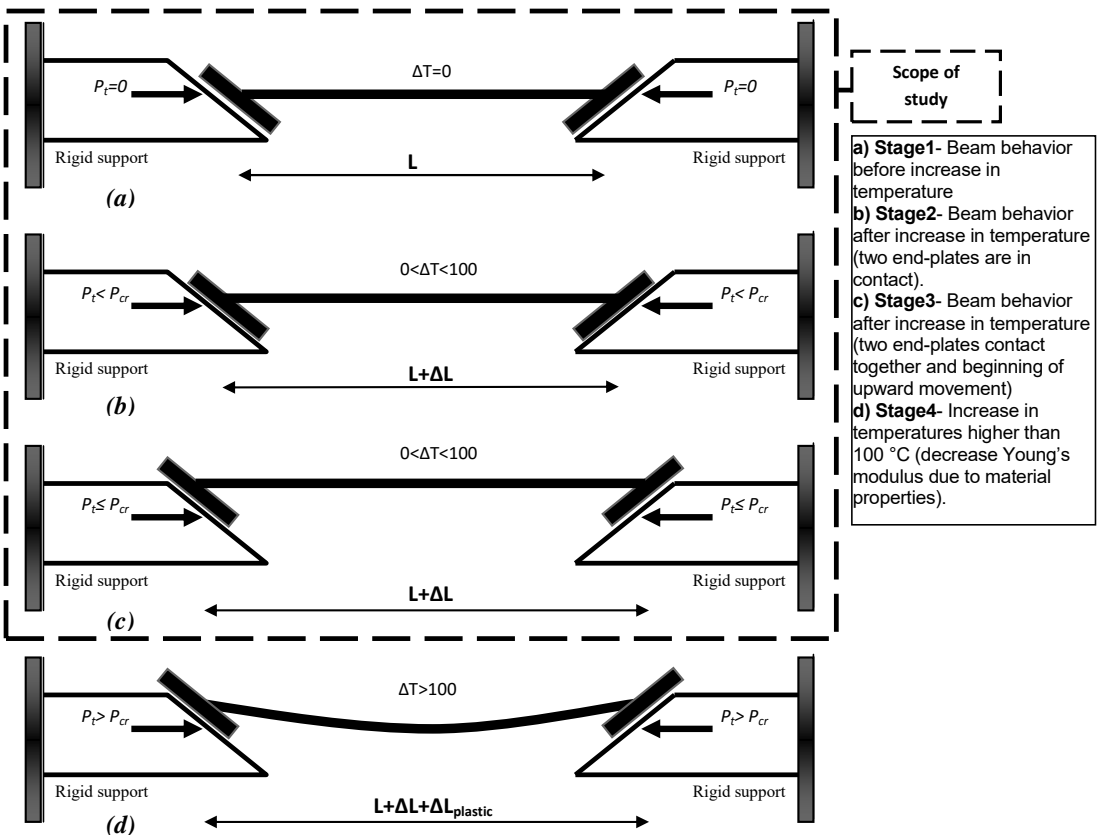

Figure 4: Beam with slant end-plate connection subjected to temperature increase.

3 DIRECT STIFFNESS FINITE ELEMENT FORMULATION

3.1 Case Study Description

In the current formulation, three case studies are simulated in two common categories; before thermal effect and after uniform elevated temperature. In the first case study, it is assumed that the two ends of the beam are supported with rollers on a fixed slanting plane that can carry the moment. The second case study is similar to the first case but its difference is there exists now a friction force between the two end-plates. In the third case study, we consider the use of the friction bolts in the beam with slant end-plate connection. The effects of various types of friction factors and slanting angles are to be investigated. The results from the direct stiffness formulation are first validated by an experimental test for selected cases. To expand study to all cases, results from the direct stiffness method and the modeling using the commercial finite element package, ABAQUS 6.9, are compared with those of analytical equations given by Zahmatkesh et al. (2014b).

3.2 The Connection with Roller Supports

For convenience, the joints of end-plate connections in the current case are assumed to be rigid. In addition, the ends of the lower part of slanting line are prevented from further downward move-

ment while the other ends are free as shown in Figure 5. The supports are rollers on slanted lines, so that the beam is in static equilibrium before thermal effect. In the static equilibrium, the uniform symmetric transverse load, *W*, causes the roller end-plates to move downward, but the initial axial load in the beam, *Pi*, resists against downward sliding. Therefore, in this case study, if any compression axial force due to elevated temperature is applied, the end-plates tend to move upward without any resistive force from support reaction such as friction. The boundary condition (B.C.) of roller supports can channel the total elongation of beam by free sliding upward over the slanting surface. As a result, the amount of axial force due to elevated temperature goes to zero and is damped completely. For model description, the beam member in Figure 5 is divided into two elements and three joints (nodes) such that the length of each element is equal to *L* with the same properties of section (cross-sectional area, *A*, and second moment of area, *I*) and material (Young's modulus, *E*). For convenience of displacements and reaction forces computations, local axes definitions that follow the slant plane are adopted: X1-Y1 at the left and X3-Y3 at the right hand sides and X2-Y2 local axes at node 2 that is coincided with the global axes. From the standard stiffness matrix of general frame element, $K_{element}$, and the transformation matrices, *T1* and *T2*, the stiffness matrices of elements, *K1* and *K2*, at local axes can be obtained from Equations 1 and 2. Note that local axes are used instead of global axes to obtain force and displacement at the slanting direction. The angle of beam element with the left support in the X1-Y1 local axes is equal to θ_1, and it is equal to θ_3 at the right support in the X3-Y3 local axes. In the model, the angle of end-plate with the vertical on the left hand side is considered similar to that of the right hand side (θ).

$$\left[K_1\right]=\left[T_1\right]^T\left[K\right]\left[T_1\right] \tag{1}$$

$$\left[K_2\right]=\left[T_2\right]^T\left[K\right]\left[T_2\right] \tag{2}$$

Where

$$T_1=\begin{pmatrix} \cos\theta_1 & \sin\theta_1 & 0 & 0 & 0 & 0 \\ -\sin\theta_1 & \cos\theta_1 & 0 & 0 & 0 & 0 \\ 0 & 0 & 1 & 0 & 0 & 0 \\ 0 & 0 & 0 & \cos\theta_2 & \sin\theta_2 & 0 \\ 0 & 0 & 0 & -\sin\theta_2 & \cos\theta_2 & 0 \\ 0 & 0 & 0 & 0 & 0 & 1 \end{pmatrix} \tag{3}$$

$$T_2=\begin{pmatrix} \cos\theta_2 & \sin\theta_2 & 0 & 0 & 0 & 0 \\ -\sin\theta_2 & \cos\theta_2 & 0 & 0 & 0 & 0 \\ 0 & 0 & 1 & 0 & 0 & 0 \\ 0 & 0 & 0 & \cos\theta_3 & \sin\theta_3 & 0 \\ 0 & 0 & 0 & -\sin\theta_3 & \cos\theta_3 & 0 \\ 0 & 0 & 0 & 0 & 0 & 1 \end{pmatrix} \tag{4}$$

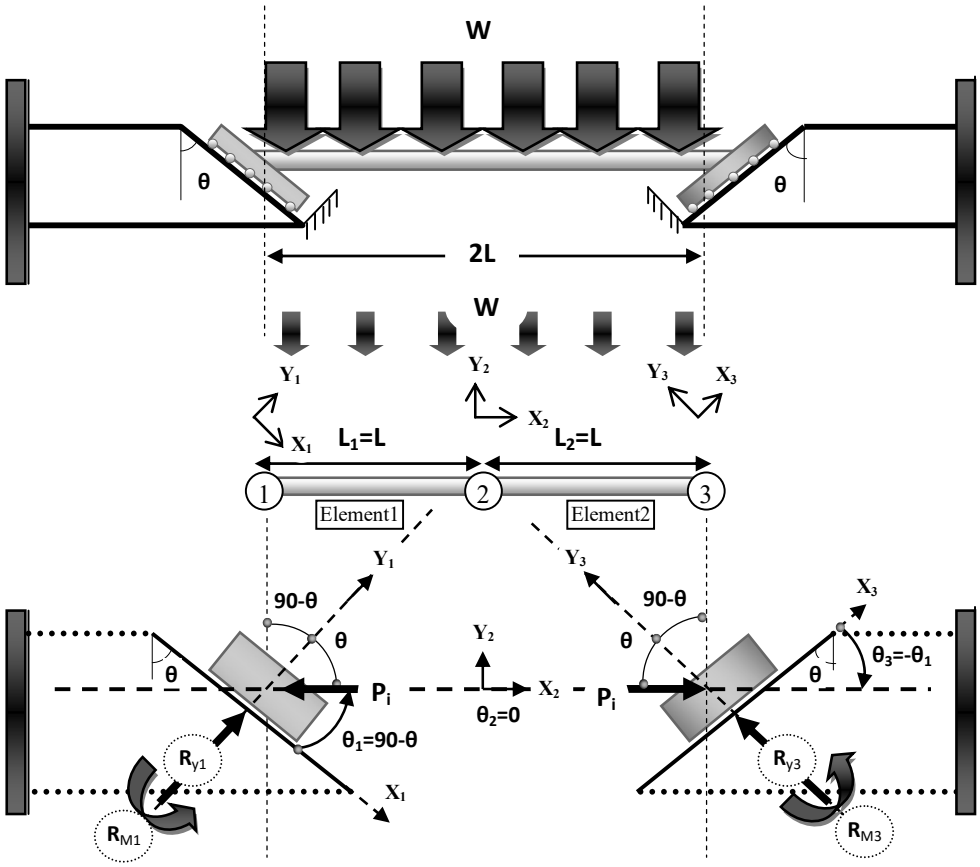

Figure 5: Force diagram of beam with slant end-plate connections due to symmetric transverse load and increase in temperature (frictionless support).

Standard stiffness matrix of general frame element:

$$K = K_{element} = \begin{pmatrix} \frac{EA}{L} & 0 & 0 & \frac{-EA}{L} & 0 & 0 \\ 0 & \frac{12EI}{L^3} & \frac{6EI}{L^2} & 0 & \frac{-12EI}{L^3} & \frac{6EI}{L^2} \\ 0 & \frac{6EI}{L^2} & \frac{4EI}{L} & 0 & \frac{-6EI}{L^2} & \frac{2EI}{L} \\ \frac{-EA}{L} & 0 & 0 & \frac{EA}{L} & 0 & 0 \\ 0 & \frac{-12EI}{L^3} & \frac{-6EI}{L^2} & 0 & \frac{12EI}{L^3} & \frac{-6EI}{L^2} \\ 0 & \frac{6EI}{L^2} & \frac{2EI}{L} & 0 & \frac{-6EI}{L^2} & \frac{4EI}{L} \end{pmatrix} \quad (5)$$

So that Equations (1) and (2) can now be written as:

$$K_1 = \begin{pmatrix} c_1^2(\frac{EA}{L}) + s_1^2(\frac{12EI}{L^3}) & c_1 s_1(\frac{EA}{L}) - c_1 s_1(\frac{12EI}{L^3}) & -s_1(\frac{6EI}{L^2}) & -c_1 c_2(\frac{EA}{L}) - s_1 s_2(\frac{12EI}{L^3}) & -c_1 s_2(\frac{EA}{L}) + c_2 s_1(\frac{12EI}{L^3}) & -s_1(\frac{6EI}{L^2}) \\ c_1 s_1(\frac{EA}{L}) - c_1 s_1(\frac{12EI}{L^3}) & s_1^2(\frac{EA}{L}) + c_1^2(\frac{12EI}{L^3}) & c_1(\frac{6EI}{L^2}) & -c_2 s_1(\frac{EA}{L}) + c_1 s_2(\frac{12EI}{L^3}) & -s_1 s_2(\frac{EA}{L}) - c_1 c_2(\frac{12EI}{L^3}) & c_1(\frac{6EI}{L^2}) \\ -s_1(\frac{6EI}{L^2}) & c_1(\frac{6EI}{L^2}) & \frac{4EI}{L} & s_2(\frac{6EI}{L^2}) & -c_2(\frac{6EI}{L^2}) & \frac{2EI}{L} \\ -c_1 c_2(\frac{EA}{L}) - s_1 s_2(\frac{12EI}{L^3}) & -c_2 s_1(\frac{EA}{L}) + c_1 s_2(\frac{12EI}{L^3}) & s_2(\frac{6EI}{L^2}) & c_2^2(\frac{EA}{L}) + s_2^2(\frac{12EI}{L^3}) & c_2 s_2(\frac{EA}{L}) - c_2 s_2(\frac{12EI}{L^3}) & s_2(\frac{6EI}{L^2}) \\ -c_1 s_2(\frac{EA}{L}) + c_2 s_1(\frac{12EI}{L^3}) & -s_1 s_2(\frac{EA}{L}) - c_1 c_2(\frac{12EI}{L^3}) & -c_2(\frac{6EI}{L^2}) & c_2 s_2(\frac{EA}{L}) - c_2 s_2(\frac{12EI}{L^3}) & s_2^2(\frac{EA}{L}) + c_2^2(\frac{12EI}{L^3}) & -c_2(\frac{6EI}{L^2}) \\ -s_1(\frac{6EI}{L^2}) & c_1(\frac{6EI}{L^2}) & \frac{2EI}{L} & s_2(\frac{6EI}{L^2}) & -c_2(\frac{6EI}{L^2}) & \frac{4EI}{L} \end{pmatrix} \tag{6}$$

$$K_2 = \begin{pmatrix} c_2^2(\frac{EA}{L}) + s_2^2(\frac{12EI}{L^3}) & c_2 s_2(\frac{EA}{L}) - c_2 s_2(\frac{12EI}{L^3}) & -s_2(\frac{6EI}{L^2}) & -c_2 c_3(\frac{EA}{L}) - s_2 s_3(\frac{12EI}{L^3}) & -c_2 s_3(\frac{EA}{L}) + c_3 s_2(\frac{12EI}{L^3}) & -s_2(\frac{6EI}{L^2}) \\ c_2 s_2(\frac{EA}{L}) - c_2 s_2(\frac{12EI}{L^3}) & s_2^2(\frac{EA}{L}) + c_2^2(\frac{12EI}{L^3}) & c_2(\frac{6EI}{L^2}) & -c_3 s_2(\frac{EA}{L}) + c_2 s_3(\frac{12EI}{L^3}) & -s_2 s_3(\frac{EA}{L}) - c_2 c_3(\frac{12EI}{L^3}) & c_2(\frac{6EI}{L^2}) \\ -s_2(\frac{6EI}{L^2}) & c_2(\frac{6EI}{L^2}) & \frac{4EI}{L} & s_3(\frac{6EI}{L^2}) & -c_3(\frac{6EI}{L^2}) & \frac{2EI}{L} \\ -c_2 c_3(\frac{EA}{L}) - s_2 s_3(\frac{12EI}{L^3}) & -c_3 s_2(\frac{EA}{L}) + c_2 s_3(\frac{12EI}{L^3}) & s_3(\frac{6EI}{L^2}) & c_3^2(\frac{EA}{L}) + s_3^2(\frac{12EI}{L^3}) & c_3 s_3(\frac{EA}{L}) - c_3 s_3(\frac{12EI}{L^3}) & s_3(\frac{6EI}{L^2}) \\ -c_2 s_3(\frac{EA}{L}) + c_3 s_2(\frac{12EI}{L^3}) & -s_2 s_3(\frac{EA}{L}) - c_2 c_3(\frac{12EI}{L^3}) & -c_3(\frac{6EI}{L^2}) & c_3 s_3(\frac{EA}{L}) - c_3 s_3(\frac{12EI}{L^3}) & s_3^2(\frac{EA}{L}) + c_3^2(\frac{12EI}{L^3}) & -c_3(\frac{6EI}{L^2}) \\ -s_2(\frac{6EI}{L^2}) & c_2(\frac{6EI}{L^2}) & \frac{2EI}{L} & s_3(\frac{6EI}{L^2}) & -c_3(\frac{6EI}{L^2}) & \frac{4EI}{L} \end{pmatrix} \tag{7}$$

Where

$$c_1 = \cos\theta_1 \ , \ c_2 = \cos\theta_2 \ , \ c_3 = \cos\theta_3 \ , \ s_1 = \sin\theta_1 \ , \ s_2 = \sin\theta_2 \ , \ s_3 = \sin\theta_3 \tag{8}$$

Hence, the total equilibrium equation for the beam takes the following form.

$$\underbrace{\begin{pmatrix} K^1_{11} & K^1_{12} & K^1_{13} & K^1_{14} & K^1_{15} & K^1_{16} & 0 & 0 & 0 \\ K^1_{21} & K^1_{22} & K^1_{23} & K^1_{24} & K^1_{25} & K^1_{26} & 0 & 0 & 0 \\ K^1_{31} & K^1_{32} & K^1_{33} & K^1_{34} & K^1_{35} & K^1_{36} & 0 & 0 & 0 \\ K^1_{41} & K^1_{42} & K^1_{43} & K^1_{44}+K^2_{11} & K^1_{45}+K^2_{12} & K^1_{46}+K^2_{13} & K^2_{14} & K^2_{15} & K^2_{16} \\ K^1_{51} & K^1_{52} & K^1_{53} & K^1_{54}+K^2_{21} & K^1_{55}+K^2_{22} & K^1_{56}+K^2_{23} & K^2_{24} & K^2_{25} & K^2_{26} \\ K^1_{61} & K^1_{62} & K^1_{63} & K^1_{64}+K^2_{31} & K^1_{65}+K^2_{32} & K^1_{66}+K^2_{33} & K^2_{34} & K^2_{35} & K^2_{36} \\ 0 & 0 & 0 & K^2_{41} & K^2_{42} & K^2_{43} & K^2_{44} & K^2_{45} & K^2_{46} \\ 0 & 0 & 0 & K^2_{51} & K^2_{52} & K^2_{53} & K^2_{54} & K^2_{55} & K^2_{56} \\ 0 & 0 & 0 & K^2_{61} & K^2_{62} & K^2_{63} & K^2_{64} & K^2_{65} & K^2_{66} \end{pmatrix}}_{K_{total}} \begin{pmatrix} dx_1 \\ dy_1 \\ dr_1 \\ dx_2 \\ dy_2 \\ dr_2 \\ dx_3 \\ dy_3 \\ dr_3 \end{pmatrix} = \begin{pmatrix} Rx_1 \\ Ry_1 \\ Rm_1 \\ Rx_2 \\ Ry_2 \\ Rm_2 \\ Rx_3 \\ Ry_3 \\ Rm_3 \end{pmatrix} + \begin{pmatrix} fx_1 \\ fy_1 \\ fm_1 \\ fx_2 \\ fy_2 \\ fm_2 \\ fx_3 \\ fy_3 \\ fm_3 \end{pmatrix} \tag{9}$$

Where

$$U_{displacement\ \&\ rotation} = \begin{pmatrix} dx_1 \\ dy_1 \\ dr_1 \\ dx_2 \\ dy_2 \\ dr_2 \\ dx_3 \\ dy_3 \\ dr_3 \end{pmatrix}, \quad F_{force\ \&\ reaction} = \begin{pmatrix} Rx_1 \\ Ry_1 \\ Rm_1 \\ Rx_2 \\ Ry_2 \\ Rm_2 \\ Rx_3 \\ Ry_3 \\ Rm_3 \end{pmatrix} + \begin{pmatrix} fx_1 \\ fy_1 \\ fm_1 \\ fx_2 \\ fy_2 \\ fm_2 \\ fx_3 \\ fy_3 \\ fm_3 \end{pmatrix} \tag{10}$$

are the displacement and the force vectors, respectively.

In the current case, the B.C. are:

$$\begin{aligned} &dy_1 = 0,\ \ dr_1 = 0,\ dx_2 = 0,\ dr_2 = 0,\ dy_3 = 0,\ dr_3 = 0, \\ &Rx_1 = 0,\ Rx_2 = 0, Ry_2 = 0,\ Rm_2 = 0,\ Rx_3 = 0, \\ &fx_1 = \frac{WL}{2}\cos\theta,\ fy_1 = -\frac{WL}{2}\sin\theta,\ fm_1 = -\frac{WL^2}{12},\ fx_2 = 0,\ fy_2 = -WL,\ fm_2 = 0, \\ &fx_3 = -\frac{WL}{2}\cos\theta, fy_3 = -\frac{WL}{2}\sin\theta,\ fm_3 = \frac{WL^2}{12}, \end{aligned} \tag{11}$$

Substituting B.C. in Equation 9 and solving, we get:

$$R_{reaction} = \begin{pmatrix} Rx_1 \\ Ry_1 \\ Rm_1 \\ Rx_2 \\ Ry_2 \\ Rm_2 \\ Rx_3 \\ Ry_3 \\ Rm_3 \end{pmatrix} = \begin{pmatrix} 0 \\ \frac{WL}{\sin\theta} \\ \frac{WL^2}{3} \\ 0 \\ 0 \\ 0 \\ 0 \\ \frac{WL}{\sin\theta} \\ -\frac{WL^2}{3} \end{pmatrix} \tag{12}$$

The amount of axial force (Pi) in the beam due to symmetric transverse load and elevated temperature when frictionless supports are used can be obtained from:

$$P_i = WL\cot\theta \quad (frictionless) \tag{13}$$

3.3 The Connection with Friction Support

3.3.1 Before Elevated Temperature

In this case study, it is assumed that there is a friction force between two faces of slant end-plates at connection. So, an elastic spring stiffness, *Kg*, is used instead of friction reaction in supports at the local axes directions. As shown in Figure 6, the stiffness of this spring depends on the amount of friction factor and direction of sliding. Before any thermal effect, the beam is subjected only to symmetric transverse load. Therefore, the two end-plates with rollers tend to slide downward but the friction force that is replaced by spring, *Kg*, resists against sliding on the slant plane. In calculating the stiffness of spring, the displacements of the end-plate on slanting lines (X1 and X3) due to shortening of beam by initial axial load, *Pi*, are required.

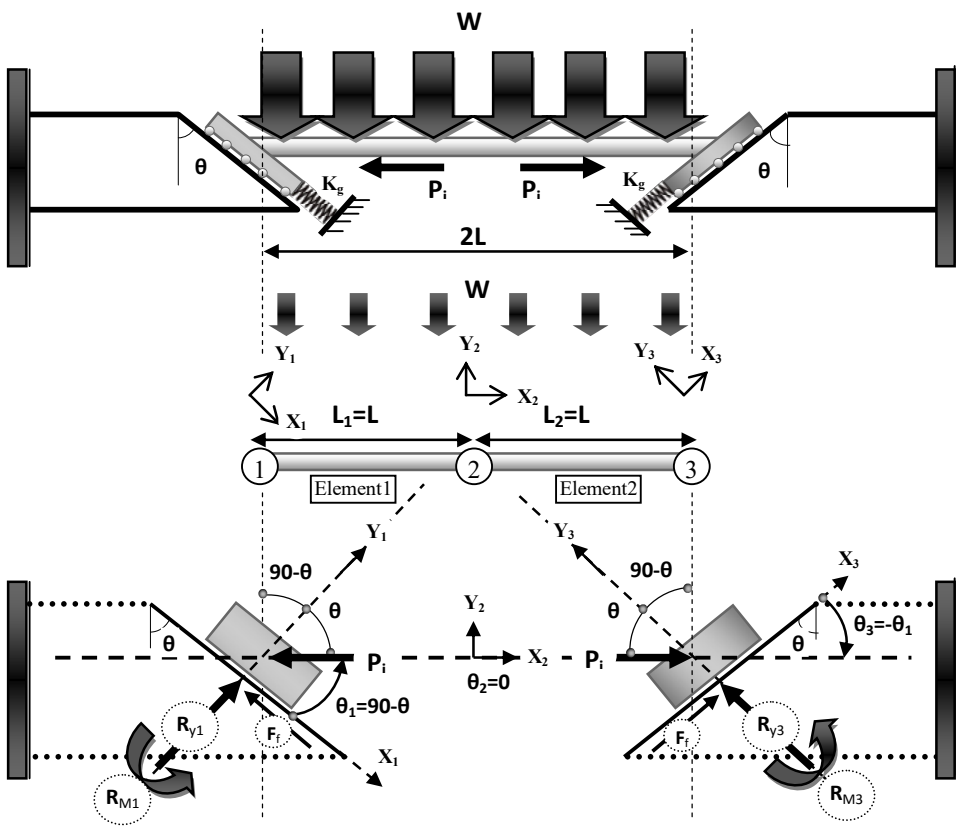

Figure 6: Force diagram of beam with slant end-plate connections due to symmetric transverse load (friction supports, before elevated temperature).

The total equilibrium relationship of such a beam can be expressed as:

$$[K_{total}]\times\begin{pmatrix} dx_1 \\ dy_1 \\ d_{rotation_1} \\ dx_2 \\ dy_2 \\ d_{rotation_2} \\ dx_3 \\ dy_3 \\ d_{rotation_3} \end{pmatrix}=\begin{pmatrix} -K_g\times dx_1 \\ Ry_1 \\ Rm_1 \\ Rx_2 \\ Ry_2 \\ Rm_2 \\ -K_g\times dx_3 \\ Ry_3 \\ Rm_3 \end{pmatrix}+\begin{pmatrix} fx_1 \\ fy_1 \\ fm_1 \\ fx_2 \\ fy_2 \\ fm_2 \\ fx_3 \\ fy_3 \\ fm_3 \end{pmatrix} \tag{14}$$

From Equation 14, it can be found that the total stiffness matrix is similar to the first case study (frictionless support). But when the friction support is used, the reaction force of spring, $K_g d_{xi}$, should be considered. After the substitution of the reaction force of spring into the reaction vector, the displacement and initial axial force due to the symmetric transverse load before thermal effect can be obtained with the following B.C.

$$\begin{aligned} &dy_1=0,\ dr_1=0,\ dx_2=0,\ \ dr_2=0,\ dy_3=0,\ dr_3=0,\\ &Rx_1=-K_g dx_1,\ Rx_2=0,\ Ry_2=0,\ Rm_2=0,\ Rx_3=-K_g dx_3,\\ &fx_1=\frac{WL}{2}\cos\theta,\ fy_1=-\frac{WL}{2}\sin\theta,\ \ fm_1=-\frac{WL^2}{12},\\ &fx_2=0,\ fy_2=-.WL,\ fm_2=0,\\ &fx_3=-\frac{WL}{2}\cos\theta,\ \ fy_3=-\frac{WL}{2}\sin\theta,\ fm_3=\frac{WL^2}{12}, \end{aligned} \tag{15}$$

and the following corresponding expressions.

Elongation of beam in the X_1 direction (frictionless case):

$$\Delta L_{x1}=\Delta L_{g-x1}=\frac{P_i(2L)}{2AE\sin\theta}=\frac{WL^2\cos\theta}{AE\sin^2\theta} \tag{16}$$

Free displacement in the X_1 direction depending on friction:

$$\Delta d_{x1}=\frac{\Delta L_{g-x1}(2f_{x1}-F_f)}{2f_{x1}} \tag{17}$$

Friction force in the slanting direction:

$$F_f=WL\left(\frac{\mu_s}{\sin\theta+\mu_s\cos\theta}\right) \tag{18}$$

Stiffness of spring in the slanting direction:

$$K_g = \frac{F_f}{\Delta d_{x1}} = \frac{AE}{L}\left(\frac{\mu_s \sin\theta}{\cos\theta - \mu_s \sin\theta}\right) \tag{19}$$

From Equation 16, the free displacement due to contraction on the slant direction at roller support can be obtained. Equation 17 shows that when there is a friction force between end-plates, the amount of such displacement will be decreased. Hence, we can use a spring to replace and cover the free downward displacement where the friction force tends to resist sliding. The stiffness of spring before thermal effect can be obtained using Equations 18 and 19.

3.3.2 After Elevated Temperature

After elevated temperature, the primary length of the beam increases but two ends of the member are axially semi-restrained. Therefore, the reaction of support induces an axial force in the beam. This axial force depends on the elevated temperature and the boundary condition at the supports. The slanting direction of supports allows the end-plates to crawl upward when the amount of initial axial load due to elevated temperature, *Pt*, is higher than the axial force only due to symmetric transverse load and friction force on the slant surface. Here, the upward resistance force (friction) is simulated by a spring stiffness, *Kt* (Figure7).

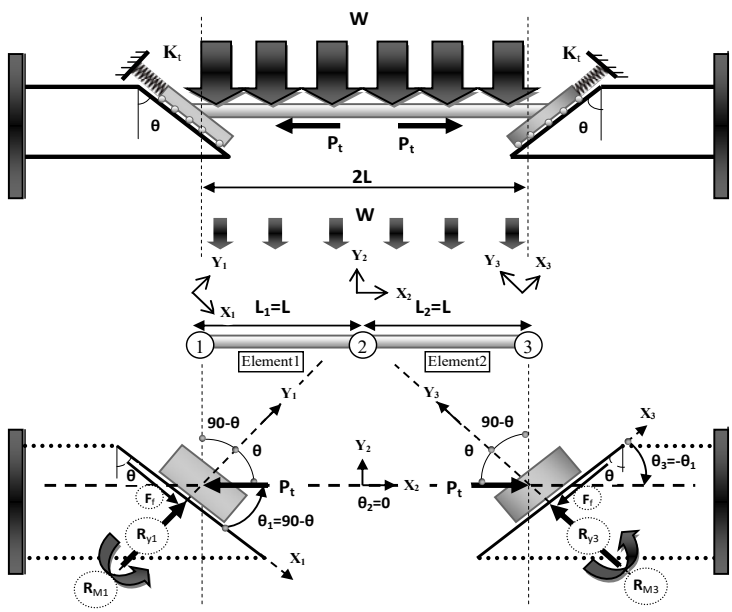

Figure 7: Force diagram of beam with slant end-plate connections due to symmetric transverse load and increase in temperature (friction support, after elevated temperature).

As shown in Figure 7, the direction of movement is upward, and the spring resists against this sliding. The total equilibrium relationship of such a beam can be expressed as:

$$[K_{total}]\times\begin{pmatrix} dx_1 \\ dy_1 \\ dr_1 \\ dx_2 \\ dy_2 \\ dr_2 \\ dx_3 \\ dy_3 \\ dr_3 \end{pmatrix}=\begin{pmatrix} -K_t\times dx_1 \\ Ry_1 \\ Rm_1 \\ Rx_2 \\ Ry_2 \\ Rm_2 \\ -K_t\times dx_3 \\ Ry_3 \\ Rm_3 \end{pmatrix}+\begin{pmatrix} fx_1 \\ fy_1 \\ fm_1 \\ fx_2 \\ fy_2 \\ fm_2 \\ fx_3 \\ fy_3 \\ fm_3 \end{pmatrix}+\begin{pmatrix} -P_t\sin\theta \\ -P_t\cos\theta \\ 0 \\ 0 \\ 0 \\ 0 \\ P_t\sin\theta \\ -P_t\cos\theta \\ 0 \end{pmatrix} \tag{20}$$

With the following corresponding important parameters.

Elongation of beam in the X_1 direction (frictionless case):

$$\Delta L_{x1}=\Delta L_{t-x1}-\Delta L_{g-x1} \tag{21}$$

Free displacement in the X_1 direction depending on friction:

$$\Delta d_{x1}=\frac{\Delta L_{x1}(P_t\sin\theta-2f_{x1}-F_f)}{P_t\sin\theta-2f_{x1}} \tag{22}$$

Friction force in the slanting direction:

$$F_f=WL\left(\frac{\mu_s}{\sin\theta-\mu_s\cos\theta}\right) \tag{23}$$

Stiffness of spring in the slanting direction:

$$K_t=\frac{F_f}{\Delta d_{x1}}=\frac{W\mathrm{AE}\mu_s\sin\theta}{AE\alpha\Delta T(\sin\theta-\mu_s\cos\theta)-WL(\cos\theta+\mu_s\sin\theta)} \tag{24}$$

From Equation 20, it can be observed that the total stiffness matrix is similar to the case of before elevated temperature, but now the reaction force of spring, K_{tdxi}, should be considered. Also, the amount of pure axial force due to elevated temperature should be added in terms of forces in the matrix equation. In calculating the stiffness of spring, Kt, the difference of the amount of shortening in the beam due to only transverse load, ΔL_{x1}, and the amount of elongation in the beam due to elevated temperature (Equation 21) should be obtained. From Equation 21, the free displacement of the end-plate on slanting plane after elevated temperature, Δ_{dx1} (Equation 22), can be computed. The stiffness of spring after uniform elevated temperature can be determined from Equations 23 and 24. After the substitution of the reaction force of spring in the reaction vector with the consideration of boundary conditions, the displacement and initial axial force due to an increase in temperature can be accordingly evaluated.

3.4 The Connection with Friction Bolt Support

3.4.1 Before Elevated Temperature

In many general end-plate connections, friction bolts are used instead of general bolts to increase the ability of connections due to sliding forces. By applying the tightening force, *Pb*, perpendicular to the slant end-plate, the friction force of bolts can be increased. This means there exists an additional resisting force against downward sliding when the beam is subjected to only symmetric transverse load. The total equilibrium relationship of such a beam can be expressed as:

$$[K_{total}]\begin{pmatrix} dx_1 \\ dy_1 \\ dr_1 \\ dx_2 \\ dy_2 \\ dr_2 \\ dx_3 \\ dy_3 \\ dr_3 \end{pmatrix} = \begin{pmatrix} -K_g \times dx_1 \\ Ry_1 \\ Rm_1 \\ Rx_2 \\ Ry_2 \\ Rm_2 \\ -K_g \times dx_3 \\ Ry_3 \\ Rm_3 \end{pmatrix} + \begin{pmatrix} fx_1 \\ fy_1 - P_b \\ fm_1 \\ fx_2 \\ fy_2 \\ fm_2 \\ fx_3 \\ fy_3 - P_b \\ fm_3 \end{pmatrix} \tag{25}$$

with the following expressions.

Elongation of beam in the X1 direction (frictionless case):

$$\Delta L_{x1} = \Delta L_{g-x1} = \frac{P_i(2L)}{2AE\sin\theta} = \frac{WL^2\cos\theta}{AE\sin^2\theta} \tag{26}$$

Free displacement in the X1 direction depending on friction:

$$\Delta d_{x1} = \frac{\Delta L_{g-x1}(2f_{x1} - F_f)}{2f_{x1}} \tag{27}$$

Friction force in the slanting direction:

$$F_f = (WL)\frac{\mu_s(WL + P_b\sin\theta)}{\sin\theta + \mu_s\cos\theta} \tag{28}$$

Stiffness of spring in the slanting direction:

$$K_g = \frac{F_f}{\Delta d_{x1}} = \frac{AE}{L}\left(\frac{\mu_s(WL\sin\theta + P_b\sin^2\theta)}{WL\cos\theta - \mu_s(WL\sin\theta + P_b)}\right) \tag{29}$$

From Equation 28, the decrease in initial axial force in the beam before any thermal effect due to the friction bolts can be determined. Here, an elastic spring, *Kg*, is used to simulate the free displacement of end-plate on the slant plane due to the transverse load. As shown in Figure 8, initiat-

ing from equilibrium, Equation (25), the stiffness of simulated spring, *Kg*, can be obtained from Equation (29).

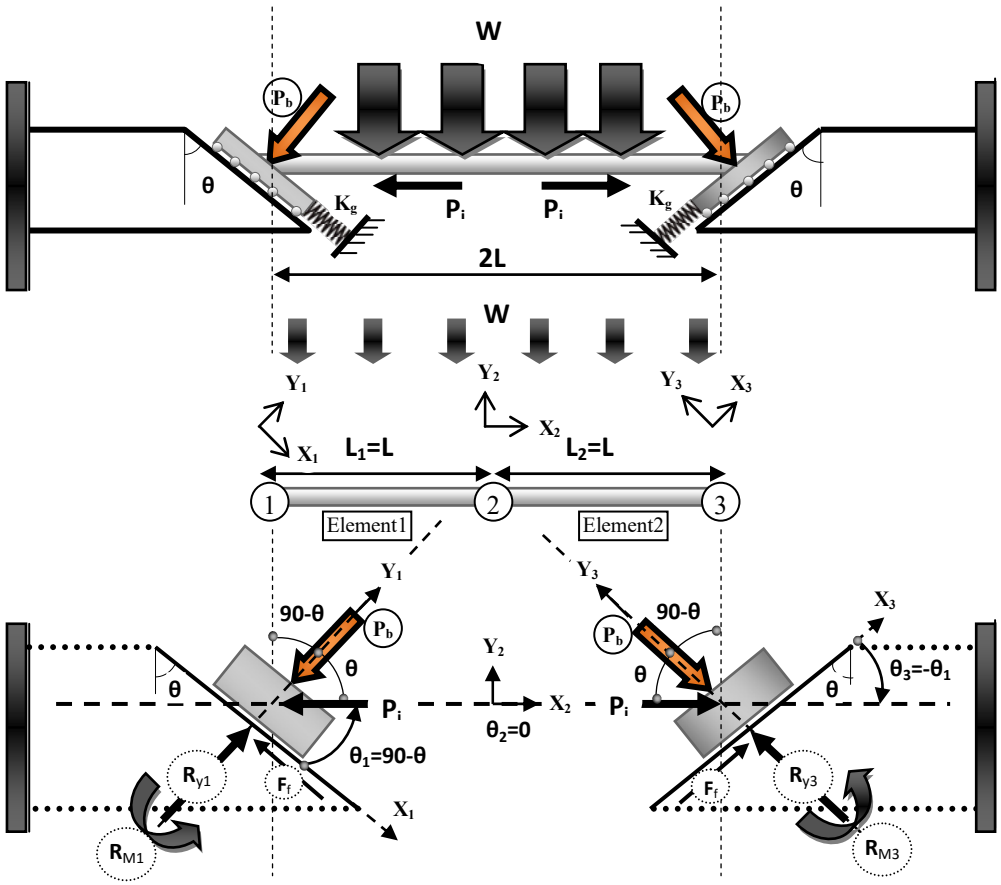

Figure 8: Force diagram of beam with slant end-plate connections due to symmetric transverse load (with friction bolts, before elevated temperature).

3.4.2 After Elevated Temperature

When the friction bolts are used in the case of after elevated temperature, the two end-plate connections tend to resist against upward movement compared with friction support with general bolts, because the amount of friction force is increased by perpendicular force that is resulted from the tightening of friction bolts. In the thermal case, the friction force changes its direction downward to set equilibrium. The total equilibrium relationship of such a beam can be expressed as Equations 30-34. As shown in Figure 9, the friction and free displacement due to elevated temperature are simulated by spring, *Kt*, from which the reaction of this spring would tend to resist against upward sliding. The minimum required initial axial force, *Pt*, to initiate the sliding with the amount of stiffness simulated by the spring, *Kt*, in this case is resulted from Equation 34.

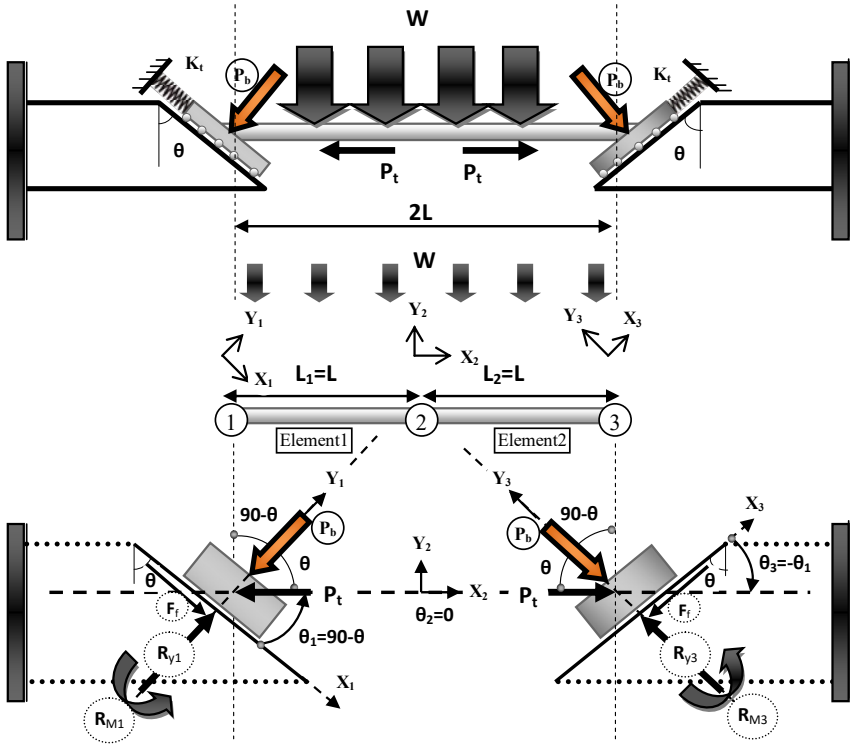

Figure 9: Force diagram of beam with slant end-plate connections due to symmetric transverse load and increase in temperature (with friction bolts, after elevated temperature).

$$[K_{total}]\begin{pmatrix} dx_1 \\ dy_1 \\ dr_1 \\ dx_2 \\ dy_2 \\ dr_2 \\ dx_3 \\ dy_3 \\ dr_3 \end{pmatrix} = \begin{pmatrix} -K_t \times dx_1 \\ Ry_1 \\ Rm_1 \\ Rx_2 \\ Ry_2 \\ Rm_2 \\ -K_t \times dx_3 \\ Ry_3 \\ Rm_3 \end{pmatrix} + \begin{pmatrix} fx_1 \\ fy_1 - P_b \\ fm_1 \\ fx_2 \\ fy_2 \\ fm_2 \\ fx_3 \\ fy_3 - P_b \\ fm_3 \end{pmatrix} + \begin{pmatrix} -P_t \sin\theta \\ -P_t \cos\theta \\ 0 \\ 0 \\ 0 \\ 0 \\ P_t \sin\theta \\ -P_t \cos\theta \\ 0 \end{pmatrix} \tag{30}$$

along with the following expressions.

Elongation of beam in the X_1 direction (frictionless case):

$$\Delta L_{x1} = \Delta L_{t-x1} - \Delta L_{g-x1} \tag{31}$$

Free displacement in the X_1 direction depending on friction:

$$\Delta d_{x1} = \frac{\Delta L_{x1}(P_t \sin\theta - 2f_{x1} - F_f)}{P_t \sin\theta - 2f_{x1}} \tag{32}$$

Friction force in the slanting direction:

$$F_f = WL\left(\frac{\mu_s(WL + P_b\sin\theta)}{\sin\theta - \mu_s\cos\theta}\right) \tag{33}$$

Stiffness of spring in the slanting direction:

$$K_t = \frac{\frac{AE}{L}\mu_s\sin\theta(WL + P_b\sin\theta)}{AE\alpha\Delta T(\sin\theta - \mu_s\cos\theta) - WL(\cos\theta - \mu_s\sin\theta) - \mu_s P_b} \tag{34}$$

4 EXPERIMENTAL TESTS AND COMPARISON WITH DIRECT STIFFNESS FORMULATION RESULTS

The structural responses computed with the direct stiffness method are first validated with experimental results. Experimental data was taken from small scale steel beam and frame tests carried out at the Faculty of Civil Engineering of Universiti Teknologi Malaysia (UTM). The geometrical details for the considered structure are shown in Figure 10. H sections with a thickness of 1.5 mm were employed for beam and columns. The height of columns and beam's length of 235 mm and 450 mm were considered, respectively.

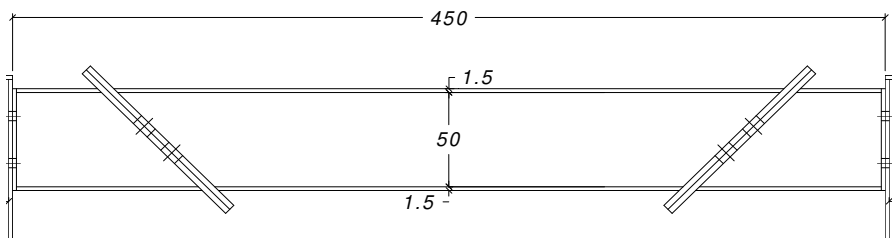

Figure 10: Geometrical details of the slant end-plate connection in a beam-to-column system for experimental study (all units are in mm).

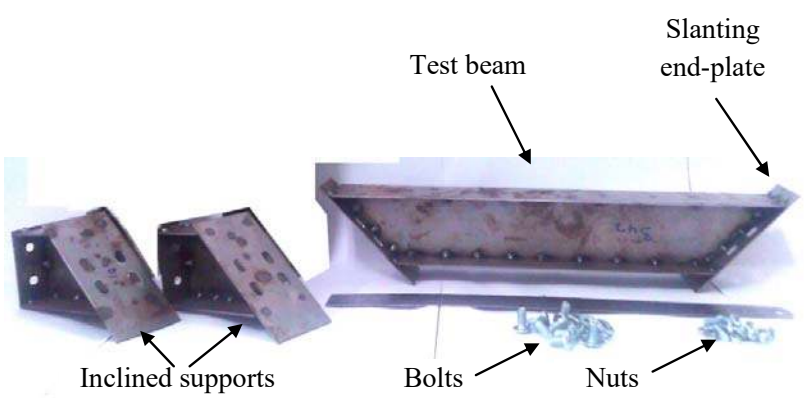

Figure 11: Parts of frame with slant end-plate connection used in the experimental study.

Figure 11 shows the composition of components used in the experimental study. The structure consists of five separated parts; two columns, two short side beams and a middle beam with two inclined ends. These five parts were assembled by normal bolts and nuts. For the tests, the side beams and middle beam were detached as separate components from the main frame, resembling those of the analytical assumptions. The slant end-plate connection can damp thermal axial force by motion on slant surface, so in the experimental model, the holes on slant end-plate connection were constructed such that they are of oval shape to allow this deformation. According to direct stiffness equations, the friction factor, μs, between two faces of slant end-plate connection joint is desired. So, a basic test was conducted to determine this as shown in Figure 12. In the friction test the self-weight of beam is measured 6.67 N with a connection slanting angle of 45° ($\theta = 45°$).

A 39.22 N attachment weight was used on the top of side beam in the vertical position. To measure the amount of sliding force, a load cell with 50 kA- 5 kN capability was located at the side of the beam. An automated data logger (UCAM-70A) was used to measure the corresponding axial force. The basic test measured a magnitude of 0.37 ($\mu s = \tan \varphi$) for the static friction factor of the inclined surfaces. After the determination of the friction factor, two additional tests; before and after elevated temperature, were carried out for measuring the structural performance of the current connection system. The test set-up can be seen in Figure 13 where the beam was tested with seven symmetric gravity load intensities (6.67 N, 26.29 N, 45.91 N, 65.53 N, 85.15 N, 104.77 and 124.39 N) including beam self-weight. Similar to the basic test, the axial force is recorded using the data logger with a load cell located at the end of the beam. For controlling the temperature under 100° (elastic zone) (EC3, 2005), ten thermocouples were attached along the beam with the heat source coming from a hot air blower placed at the middle of the beam. Note that Equations (14) and (20) from the model with the friction support assumption are specifically employed to produce the numerical results, to be compared to experimental responses.

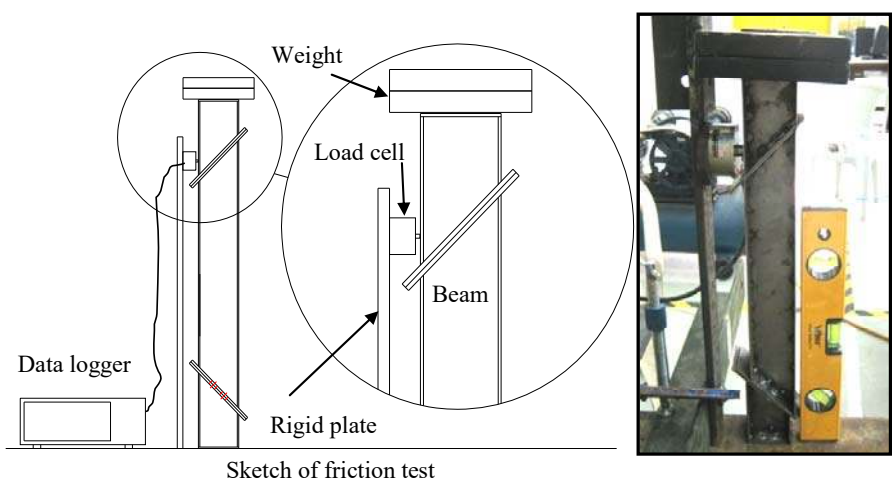

Figure 12: Basic test for finding the static friction factor (μs) between two faces of slant end-plate connection.

The relationships between applied load and the amount of axial force in the beam for the investigated two cases are shown in Figure 14. It is evident that the direct stiffness model conforms ac-

ceptably to the outcomes produced by experiments, both before and after temperature increase, and thus validating the applicability of the current numerical method.

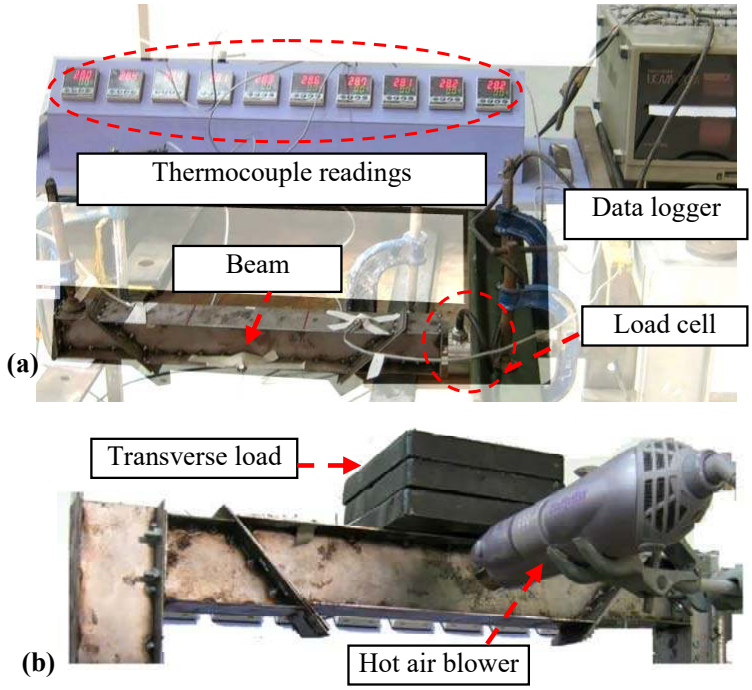

Figure 13: a) Thermal test set-up and b) method of applying temperature increase.

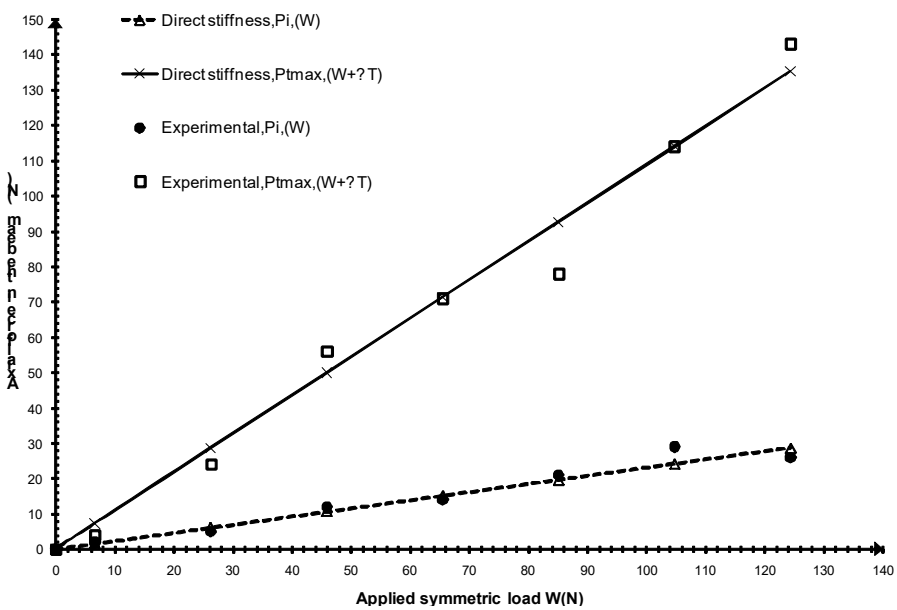

Figure 14: The relationship between symmetric load and axial force in the beam (friction factor, $\mu s = \tan \varphi = 0.37$, $\theta = 45°$).

5 NUMERIC PARAMETER STUDY

After a good agreement with experimental outcomes, we demonstrate next using the model approach the evaluation of the minimum requirement of initial axial force for equilibrium that initiates the motion at the two ends of the beam for several parametric changes. Also, the corresponding minimum elevated temperatures for end-plate crawling are computed. The structural model described in the previous section has been used to analyze a steel beam section at elevated temperature, in which an I-section (build-up) beam is connected at its ends to slant fixed end-plate supports (Figure 15). For demonstration purpose we have set for the beam: cross section area (A) = 14000 mm^2, modulus of elasticity (E) = 200 kN/mm^2, ambient temperature (T_0) = 20°C, elevated temperature (ΔT) = 50°C, length of beam (L) = 6000 mm, coefficient of thermal expansion (α) = 1.5 × 10-5 $°C^{-1}$, linear symmetric transverse load (W) = 10 kN/m, and the perpendicular axial force (tightening force) on the friction bolts (*Pb*) = 50 kN (total force). The slope of slant end-plate connection (θ) and the friction coefficient factor ($\mu s = \tan \varphi$) are varied.

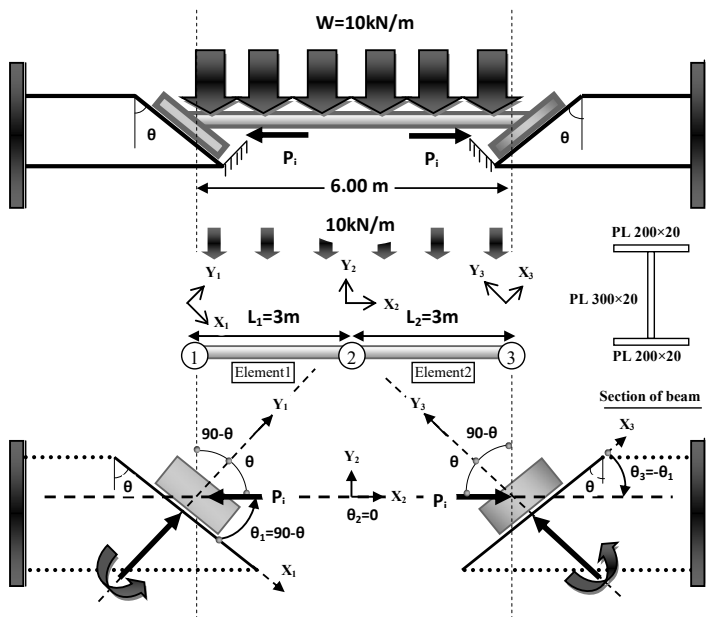

Figure 15: Numerical model geometrical detail.

In addition, a two dimensional numerical finite element model is created using the commercially available software, ABAQUS, for comparison. In the ABAQUS model, the slant support components are modeled using the continuum tetrahedral brick elements and the beam is constructed using the beam element. The contacts between end-plates are simulated by the node-to-surface formulation. For this illustration, we have considered four angles (θ = 15°, 30°, 45°, 60°) using three different friction factors (μs= 0.2, 0.3, 0.5). The results of one sample study where θ = 30° and μs is 0.2 are shown in Figure 16 for 4 cases: Using general bolts and friction bolts for each case of before and after elevated temperature. The force diagram shows that the amount of axial force due to symmetric transverse load before any thermal effect (Pi,W) is equal to 33.61 kN, but when

friction bolts are used (Pi,W+Pb), the amount of axial force decreases to 18.89 kN. It is demonstrated in Figure 16 that the friction bolts can decrease the induced axial force in the beam before elevated temperature due to just symmetric transverse load. After temperature change, the minimum requirement of axial force in the beam for initiation of crawling (Pi,W+ΔT) is equal to 86.54 kN, and when the friction bolt is used, the minimum requirement (Pi,W+Pb+ΔT) is 116.46 kN, which is higher. Also, from the results of other cases of after elevated temperature for various angles, it can be found that if the friction bolt is used instead of general bolts, a higher axial force is required to initiate crawling of the beam on the slant plane. The detail is shown next.

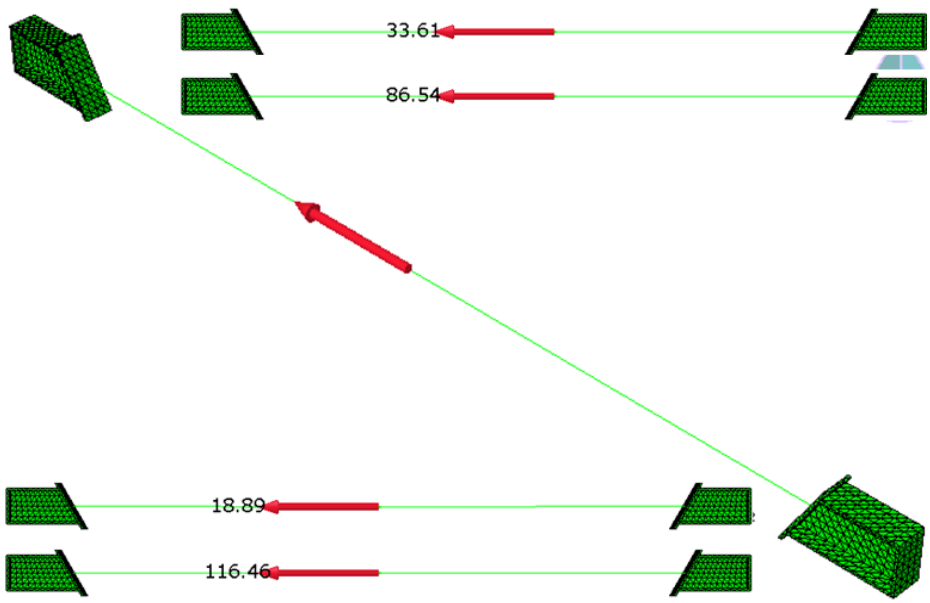

Figure 16: Schematics of ABAQUS model with arrows denoting the axial force for all considered cases for $\theta = 30^\circ$ and $\mu s = 0.2$. Unit of forces is kN

In Figures 17-22, results from three separate methods are given: ABAQUS software modeling, direct stiffness method and analytical method. Here, for verifying the results of two finite element methods (direct stiffness and ABAQUS software modeling), the analytical solutions for equations obtained by Zahmatkesh et al. (2014b). are used. It is obvious that the axial forces from analytical method coincide with those of direct stiffness. The results produced from ABAQUS match those analytical and numerical although some disagreements can be observed in Figures 18 and 21. Reduction in axial force, which is dependent on the use of friction bolts, can be seen when making comparison of results shown in Figures 17 and 20 in the case of temperature-free condition. Conversely, axial force increases in presence of elevated temperature when comparing the beams using general bolts with those using friction bolts. In this case, the existence of elevated temperature increases considerably the axial force when the friction bolts are employed, in consistence with the response displayed in Figure 16. Making use of the axial forces that are resulted from Figures 17-22 (after elevated temperature), the minimum elevated temperature required for upward sliding can be obtained.

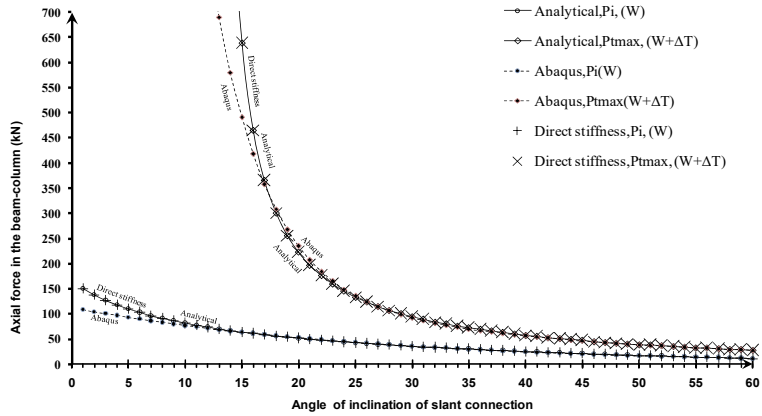

Figure 17: Relation between axial force in the beam with connection slanting (θ) subjected to symmetric transverse load and elevated temperature (friction factor, μs = tan φ = 0.2, using normal bolts)

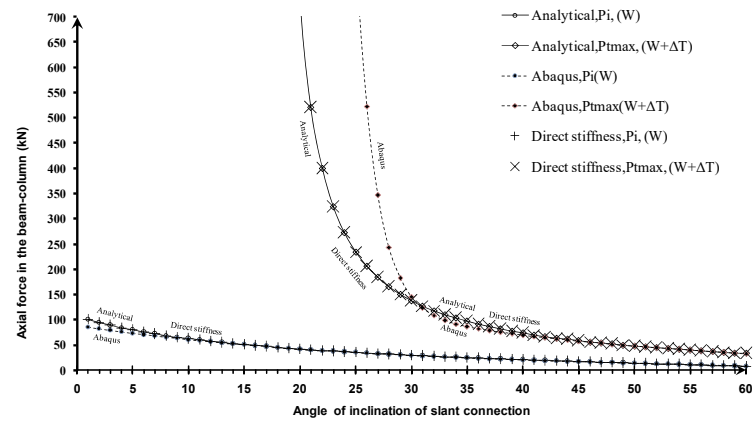

Figure 18: Relation between axial force in the beam with connection slanting (θ) subjected to symmetric transverse load and elevated temperature (friction factor, μs = tan φ = 0.3, using normal bolts)

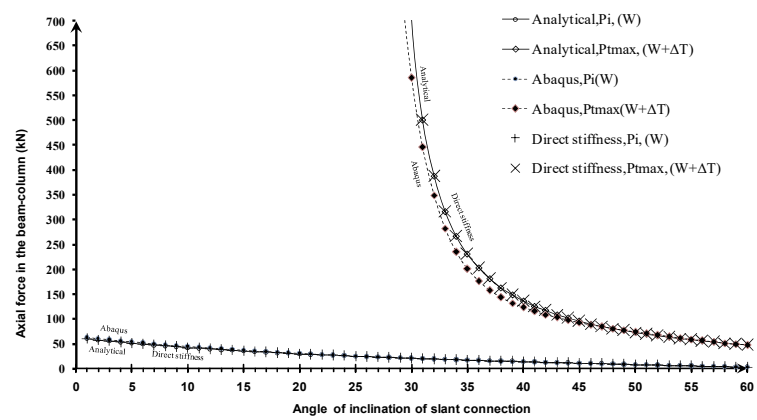

Figure 19: Relation between axial force in the beam with connection slanting (θ) subjected to symmetric transverse load and elevated temperature (friction factor, μs = tan φ = 0.5, using normal bolts)

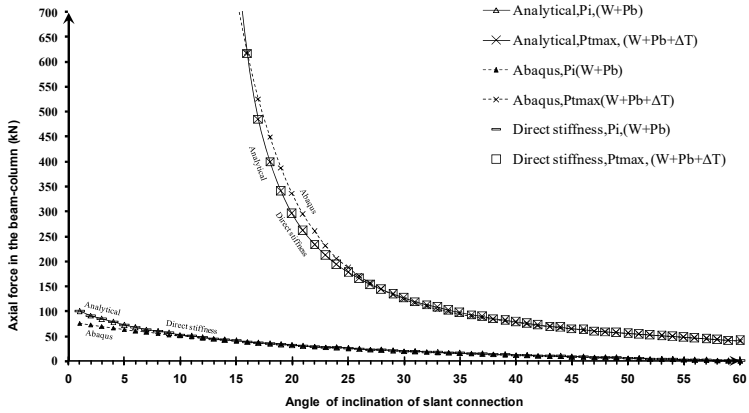

Figure 20: Relation between axial force in the beam with connection slanting (θ) subjected to symmetric transverse load and elevated temperature (friction factor, μs = tan φ = 0.2, using friction bolts)

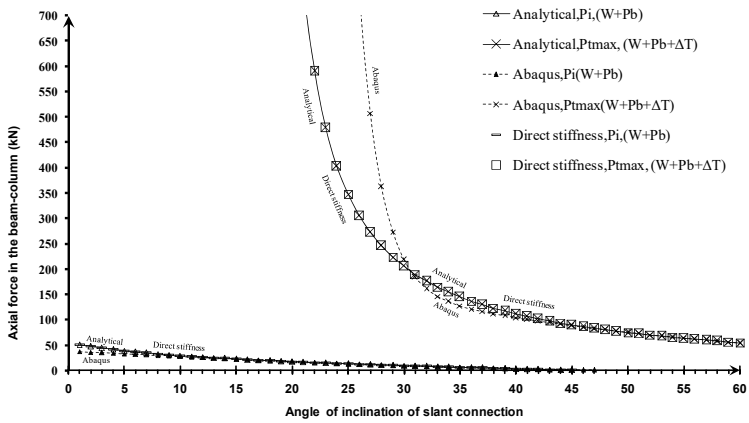

Figure 21: Relation between axial force in the beam with connection slanting (θ) subjected to symmetric transverse load and elevated temperature (friction factor, μs = tan φ = 0.3, using friction bolts)

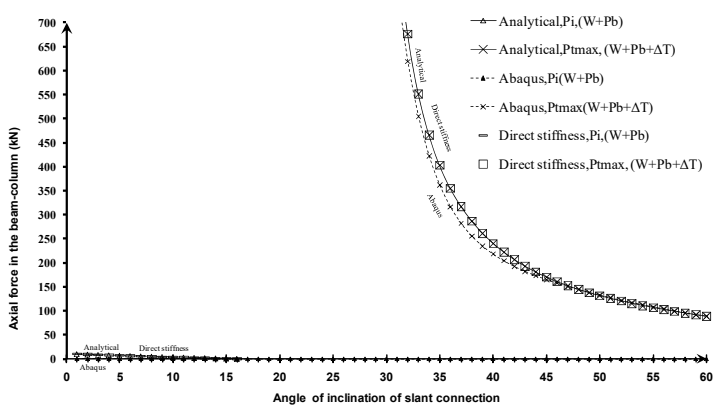

Figure 22: Relation between axial force in the beam with connection slanting (θ) subjected to symmetric transverse load and elevated temperature (friction factor, μs = tan φ = 0.5, using friction bolts)

Variation of movement initiation elevated temperatures, ΔTm, in the beam with slanting connection, θ, due to symmetric transverse load with normal and friction bolts, *Pb*, are shown in Figures 23 and 24, respectively. Again, three separate methods are used and compared. The curves of direct stiffness method match perfectly those of analytical method whereas the curves from ABAQUS model although diverge are almost parallel with them before a certain minimum inclination angle, after which the agreements are excellent. Such divergence in response may be attributed to the contact behavior between 1D middle beam elements and the side-beam solid elements. Since it has been exhibited that analytical model, current numerical model and experimental results are closely matching, the divergence by the ABAQUS model can be related to non-conforming modeling setting that captures the structural response only after a certain minimum angle of slanted connection inclination. Between 0° to 60° of connection slanting, for direct stiffness and analytical approaches, if the angle of end-plate, ϑ, is equal to the angle of friction factor, φ, ΔTm for the beam goes to infinity. If the slant connection's angle, ϑ, is equal to 90º, tan ϑ, goes to infinity. As a result, the movement-elevated temperature, ΔTm, goes to zero. This means that if the end-plate approaches the vertical position, the elevated temperature requirement for primary movement will approach infinity and if the end-plate approaches the horizontal position, the elevated temperature requirement for primary movement approaches zero. Making comparison between the amounts of minimum elevated temperature for movement, ΔTm, it can be found that by increasing the friction factor from zero to 0.5, the amount of minimum elevated temperature for movement, ΔTm, will be increased. This means the friction force that resists against upward crawling at the end of beam needs higher elevated temperature to initiate movement. Also, the normal force of friction bolts can increase the friction force against upward movement of the beam, causing increase in both axial force and ΔTm.

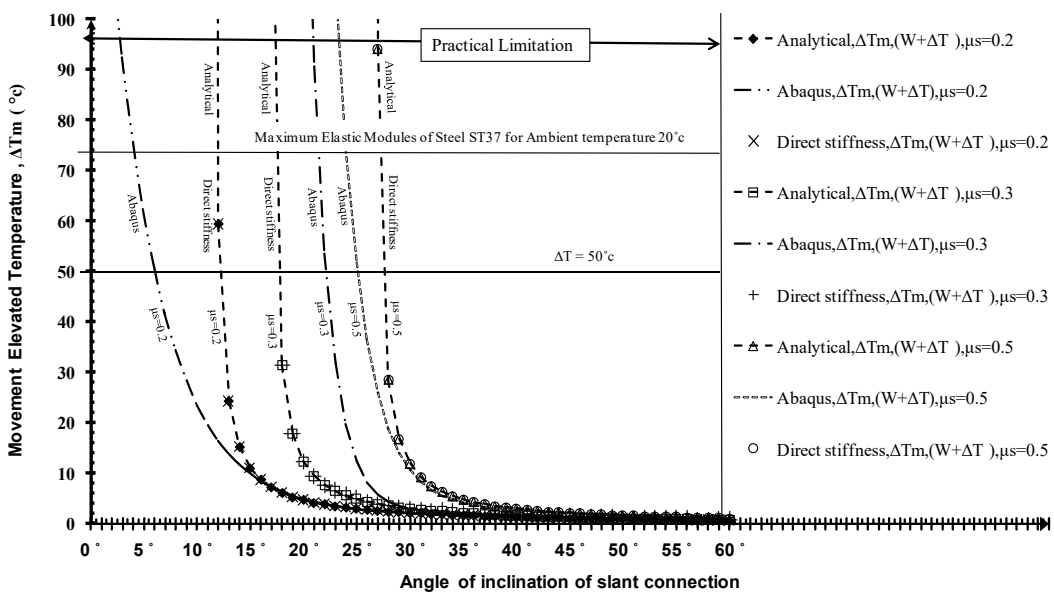

Figure 23: Relation between movement initiation elevated temperature, ΔTm, and angle of slant connection subjected to symmetric transverse load and elevated temperature (in the case of normal bolts)

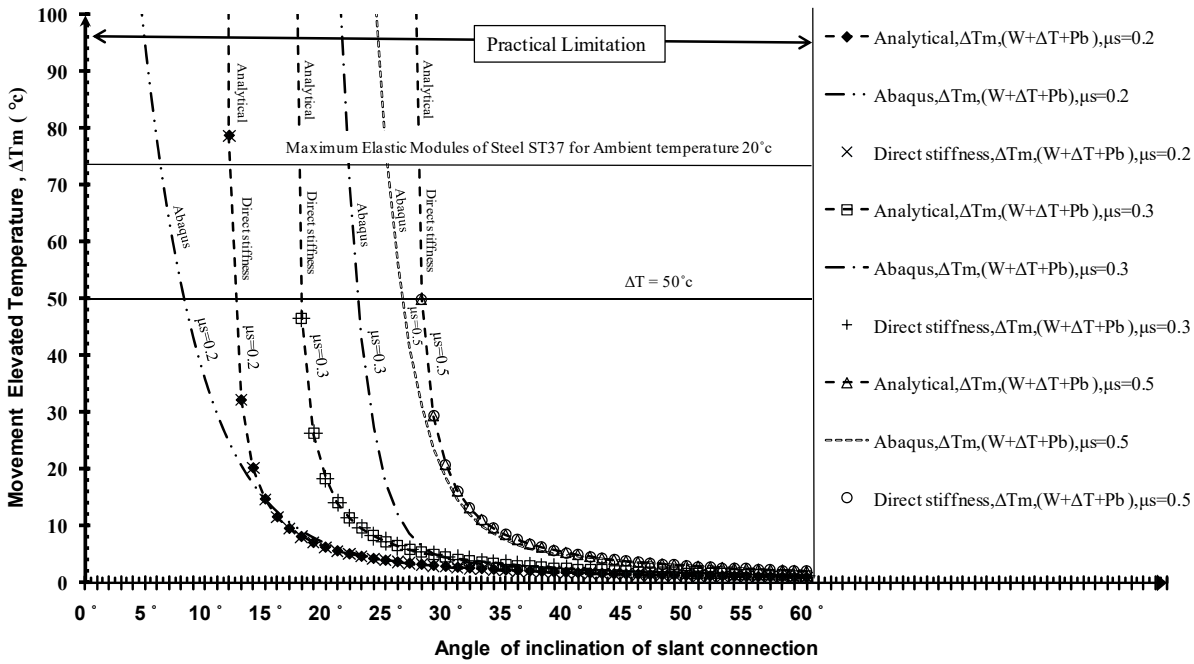

Figure 24: Relation between movement initiation elevated temperature, ΔTm, and angle of slant connection subjected to symmetric transverse load and elevated temperature (in the case of friction bolts)

6 CONCLUSION

This paper reports on the development of a linear one dimensional finite element model of the steel beam with a slant end-plate connection by means of direct stiffness matrix method and ABAQUS software modeling when it is subjected to a uniform elevated temperature (under 100° C and elastic field of steel material under thermal conditions applicable to an early stage of fire incident) and a symmetric transverse load. It has been shown that the current formulation agrees excellently in terms of the elastic structural response with the conducted test results. From the comparison of results of the direct stiffness model with those of analytical, it is demonstrated that the numerical models are able to estimate practically identical amount of initial axial force and elevated temperature for initiation of movement of a steel beam when a slant end-plate is used as connection. The parametric investigation shows that the thermal expansion of the restrained beam may cause higher axial force that can reduce the primary strength of the beam element. It is found that by changing connections' detail using the slant end-plate connection replacing that of vertical, the induced axial force is damped by the actions of friction sliding and movement on the slope surface of end-plate. Increase in the friction of end-plates contributes to a rise in the axial force in the beam. The use of friction bolts reduces the axial force in the beam in contrast to that using general bolts in absence of elevated temperature. It occurs conversely when the beams are exposed to elevated temperature.

From the models, it has been shown that the minimum requirement of elevated temperature for crawling at the end of beam, ΔTm, increases when the amount of friction factor changes from zero to 0.5 (with the increase of the friction resistance), because the friction force resists against upward crawling of the ends of beam. In the case where the friction bolts are used in presence of elevated

temperature, the friction bolts increase the friction force against upward movement of the beam, and thus increasing ΔTm. It is notable to see that by varying the symmetric transverse load, the friction factor, the inclination of the end-plate, and the normal force of friction bolts using the present model, we can potentially obtain the optimum design that has enough ability to absorb the huge axial force induced due to temperature increase in the beam before any yielding and buckling can occur.

NOMENCLATURE

$\boldsymbol{A}$ *Cross section of beam*

$\boldsymbol{E}$ *Young's modulus*

$\boldsymbol{F_f}$ *Friction force*

$\boldsymbol{I}$ *Moment of inertia*

$\boldsymbol{K_g}$ *Stiffness of simulated spring due to transverse load*

$\boldsymbol{K_t}$ *Stiffness of simulated spring due to elevated temperature*

$\boldsymbol{L}$ *Length of the beam*

$\boldsymbol{M}$ *Bending moment*

$\boldsymbol{P_b}$ *Total force of tightening in friction bolts*

$\boldsymbol{P_{cr}}$ *Critical compressive axial load*

$\boldsymbol{A}$ *Cross section of beam*

$\boldsymbol{E}$ *Young's modulus*

$\boldsymbol{F_f}$ *Friction force*

$\boldsymbol{I}$ *Moment of inertia*

$\boldsymbol{K_g}$ *Stiffness of simulated spring due to transverse load*

$\boldsymbol{K_t}$ *Stiffness of simulated spring due to elevated temperature*

$\boldsymbol{L}$ *Length of the beam*

$\boldsymbol{M}$ *Bending moment*

$\boldsymbol{P_b}$ *Total force of tightening in friction bolts*

$\boldsymbol{P_{cr}}$ *Critical compressive axial load*

References

AISC (2013). AISC Design Guide 27: Structural Stainless Steel. Institute of Steel Construction

Al-Jabri K.S. (2011). Modelling and simulation of beam-to-column joints at elevated temperature: A review. *Journal of the Franklin Institute* 348(7): 1695-1716.

Bailey C.G., Burgess I.W., Plank R.J. (1996). Analyses of the effects of cooling and fire spread on steel-framed buildings. *Fire Safety Journal* 26(4): 273-293.

Bradford M. (2006). Elastic Analysis of Straight Members at Elevated Temperatures. *Advances in Structural Engineering* 9(5): 611-618.

Chen J., Young B. (2006). Stress–strain curves for stainless steel at elevated temperatures. *Engineering Structures* 28(2): 229-239.

Dai X.H., Wang Y.C., Bailey C.G. (2010). Numerical modelling of structural fire behaviour of restrained steel beam–column assemblies using typical joint types. *Engineering Structures* 32(8): 2337-2351.

EC3 (2005). Eurocode 3 (EC3), BS EN 1993-1-2: Design of Steel Structures, Part 1-2: General Rules-Structural Fire Design. . British Standards Institution London, UK.

Heidarpour A., Bradford M.A. (2009). Elastic behaviour of panel zone in steel moment resisting frames at elevated temperatures. *Journal of Constructional Steel Research* 65(2): 489-496.

Larson S.C., Van Geem M.G. (1987). Structural thermal break systems for buildings: Feasibility study: Final report. Other Information: Portions of this document are illegible in microfiche products. Original copy available until stock is exhausted. p. Medium: X; Size: Pages: 102.

Mourão H.D.R., E Silva V.P. (2007). On the behaviour of single-span steel beams under uniform heating. *Journal of the Brazilian Society of Mechanical Sciences and Engineering* 29(1): 115-122.

Qian Z.H., Tan K.H., Burgess I.W. (2008). Behavior of steel beam-to-column joints at elevated temperature: Experimental investigation. *Journal of Structural Engineering* 134(5): 713-726.

Rodrigues J.P.C., Cabrita Neves I., Valente J.C. (2000). Experimental research on the critical temperature of compressed steel elements with restrained thermal elongation. *Fire Safety Journal* 35(2): 77-98.

Simões da Silva L., Santiago A., Vila Real P. (2001). A component model for the behaviour of steel joints at elevated temperatures. *Journal of Constructional Steel Research* 57(11): 1169-1195.

Takagi J., Deierlein G.G. (2007). Strength design criteria for steel members at elevated temperatures. *Journal of Constructional Steel Research* 63(8): 1036-1050.

Usmani A.S., Rotter J.M., Lamont S., Sanad A.M., Gillie M. (2001). Fundamental principles of structural behaviour under thermal effects. *Fire Safety Journal* 36(8): 721-744.

Yang B., Tan K.H. (2012). Numerical analyses of steel beam-column joints subjected to catenary action. *Journal of Constructional Steel Research* 70: 1-11.

Yin Y.Z., Wang Y.C. (2004). A numerical study of large deflection behaviour of restrained steel beams at elevated temperatures. *Journal of Constructional Steel Research* 60(7): 1029-1047.

Zahmatkesh F., Osman M.H., Talebi E. (2014a). Thermal Behaviour of Beams with Slant End-Plate Connection Subjected to Nonsymmetric Gravity Load. *The Scientific World Journal* 2014.

Zahmatkesh F., Osman M.H., Talebi E., Kueh A.B.H. (2014b). Analytical study of slant end-plate connection subjected to elevated temperatures. *Steel and Composite Structures* 17(1): 47-67.

Zahmatkesh F., Osman M.H., Talebi E., Kueh A.B.H. (2014c). Direct stiffness model of slant connection under thermal and non-symmetric gravity load. *Journal of Constructional Steel Research* 102(0): 24-43.